Transport of launched cold atoms with a laser guide and pulsed magnetic fields

2006 New J. Phys. 8 309

(http://iopscience.iop.org/1367-2630/8/12/309)

New Journal of Physics
The open-access journal for physics

Transport of launched cold atoms with a laser guide and pulsed magnetic fields

Matthew J Pritchard[1], **Aidan S Arnold**[2], **Simon L Cornish**[1], **David W Hallwood**[3], **Chris V S Pleasant**[1], **Ifan G Hughes**[1,4]

[1] Department of Physics, Rochester Building, University of Durham, South Road, Durham DH1 3LE, UK
[2] SUPA, Department of Physics, University of Strathclyde, Glasgow G4 0NG, UK
[3] Department of Physics, Clarendon Laboratory, Parks Road, Oxford OX1 3PU, UK
E-mail: i.g.hughes@durham.ac.uk

New Journal of Physics **8** (2006) 309
Received 4 October 2006
Published 7 December 2006
Online at http://www.njp.org/
doi:10.1088/1367-2630/8/12/309

Abstract. We propose the novel combination of a laser guide and magnetic lens to transport a cold atomic cloud. We have modelled the loading and guiding of a launched cloud of cold atoms with the optical dipole force. We discuss the optimum strategy for loading typically 30% of the atoms from a magneto-optical trap (MOT) and guiding them vertically through 22 cm. However, although the atoms are tightly confined transversely, thermal expansion in the propagation direction still results in a density loss of two orders of magnitude. By combining the laser guide with a single impulse from a magnetic lens we show one can actually increase the density of the guided atoms by a factor of 10.

[4] Author to whom any correspondence should be addressed.

PII: S1367-2630(06)34327-3

Contents

1. Introduction **2**
2. Laser guiding **4**
2.1. Modelling . . . 4
2.2. The dipole force . . . 4
2.3. Loading the guide . . . 5
2.4. Transport losses . . . 7
3. Magnetic focusing theory **9**
3.1. The Stern–Gerlach force . . . 9
3.2. Magnetic fields from current-carrying coils . . . 9
3.3. Pulse timing . . . 11
4. Laser guiding and magnetic focusing **12**
4.1. Axial only focusing . . . 13
4.2. Axial focusing/radial defocusing lenses . . . 14
4.3. Transported cloud properties . . . 17
5. Discussion and conclusion **17**
5.1. Lens comparison . . . 17
5.2. The 'ultimate' density . . . 18
5.3. Conclusions . . . 19
Acknowledgments **20**
References **20**

1. Introduction

Many cold atom experiments employ a double-chamber vacuum setup that is differentially pumped. The first collection chamber generally employs a high pressure ($\sim 10^{-9}$ Torr) magneto-optical trap (MOT) to collect a large number of cold atoms. These atoms are then transported to a lower pressure 'science' chamber to allow for longer trap lifetimes. The act of moving the atoms between the two regions results in an undesired density decrease unless steps are taken to counteract the atomic cloud's ballistic expansion. One approach is to catch atoms launched into the science chamber in a second MOT. However, an undesirable feature is the restriction placed on subsequent experiments by the laser beams and magnetic-field coils required to realize the second MOT. An alternative approach is to focus or guide the launched atoms such that they can be collected in a conservative trap. Efforts to confine the ballistic atomic motion in the transfer process can be broadly classified as either using the optical dipole force or the Stern–Gerlach force.

The optical dipole force arises from the gradient of the light-shift of the atomic ground state. To minimize light-induced heating, blue detuned laser light (where the atoms seek areas of lowlight intensity) or far-off resonance red-detuned light is used. Laser guiding between chambers has been achieved both in free space [1]–[3] and also within optical fibres [4]. Bose–Einstein condensates have also been transported from one chamber to another with an optical tweezer [5]. Further details of optical guiding experiments can be found in the reviews [6].

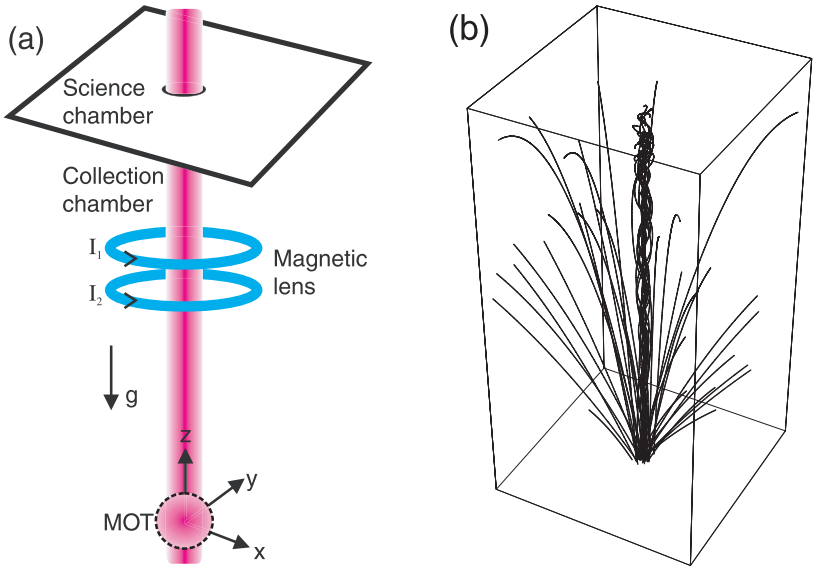

Figure 1. (a) A diagram of the experimental setup with guiding laser beam, magnetic lens and aperture for differential pumping. Atoms are collected in a MOT and then launched vertically. (b) A numerical simulation showing the trajectories of launched atoms. Roughly 30% of the atoms are guided within the laser beam, these constitute the central column of the simulation. The unguided atoms follow ballistic trajectories.

The Stern–Gerlach force can be utilized to manipulate paramagnetic cold atoms [7]. A variety of atomic mirrors for both cold [8] and Bose condensed atoms [9] have been realized. Pulsed magnetic lenses for cold atoms have also been demonstrated experimentally [10]–[12] and in recent work, we theoretically studied and optimized the designs of such lenses [13, 14].

It is also possible to load atoms into a magnetic trap in the first chamber, and transport the atoms while they are still trapped into the second chamber. Greiner *et al*'s scheme [15] involves an array of static coils, with the motion of the trapped atoms facilitated by time-dependent currents in neighbouring coils in the chain. Another scheme uses coils mounted on a motorized stage, so that they can be easily moved, thereby transporting the magnetically trapped atoms [16]. These experiments used a three-dimensional quadrupole trap, which has a magnetic zero at its centre. For certain applications a trap with a finite minimum is required, and recently transport of atom packets in a train of Ioffe–Pritchard traps was demonstrated [17].

Laser guiding effectively confines atoms in the radial direction and can have the added benefit of further cooling [2]. However, in most applications atoms remain largely unperturbed in the axial direction. In this paper, we propose a hybrid technique that combines radial confinement, via far-off resonance laser guiding, with an axially focusing magnetic lens to transport the atomic cloud, see figure 1. We investigate the optimum guiding strategy both with and without magnetic lenses.

The structure of the paper is as follows: section 2 describes how to optimize laser guiding; section 3 summarizes the theory of pulsed magnetic focusing; section 4 combines laser guiding with magnetic focusing; section 5 contains a discussion and conclusions about the results.

2. Laser guiding

2.1. Modelling

In this paper a specific experimental setup is modelled; however the analysis can be easily applied to other setups. The experimental parameters below have been chosen to be consistent with previous work at Durham University [1], [12]–[14].

Figure 1(a) shows a diagram of the guiding experiment. A MOT, centred at $\{0, 0, 0\}$, collects cold ^{85}Rb atoms at a temperature of $\mathcal{T} = 20.0\,\mu$K (with corresponding velocity standard deviation $\sigma_V = \sqrt{k_B\mathcal{T}/m} = 4.42\,\mathrm{cm\,s^{-1}}$) and with an isotropic Gaussian spatial distribution in each Cartesian direction, with standard deviation of $\sigma_R = 0.20\,$mm. The atoms are launched vertically upwards as a fountain using the moving molasses technique [18]. The initial launch velocity is chosen so that the centre of mass parabolic trajectory will have an apex at a height of $h = 22.0\,$cm above the MOT centre. This requires a launch velocity of $v_{z_i} = \sqrt{2gh} = 2.08\,\mathrm{m\,s^{-1}}$. The MOT to apex flight time is $T = \sqrt{2h/g} = 212\,$ms. At 18.0 cm above the MOT there is a 0.5 mm radius aperture to allow the atoms to pass into a lower pressure 'science' chamber (typically two orders of magnitude lower pressure). The time to reach the aperture is 121 ms for unperturbed motion.

A vertically oriented red-detuned laser provides radial guiding via the optical dipole force. The dipole trap depth is proportional to the laser power. Therefore a far-detuned guiding experiment (with negligible scattering) will always become more efficient by increasing the laser power. We have chosen to model a Nd:YAG ($\lambda_T = 1064\,$nm, subscript T used to denote the trap wavelength) guide laser that has a maximum power of 19 W. The beam waist and focal point are chosen to optimize the guiding efficiency, and this optimization process is contained in the first half of the paper.

2.2. The dipole force

For a laser, with power P, travelling along the z-axis, with a radially symmetric Gaussian transverse profile, the form of the intensity is:

$$I(r, z) = \frac{2P}{\pi w^2(z)} \exp\left(\frac{-2r^2}{w^2(z)}\right), \tag{1}$$

where $r = \sqrt{x^2 + y^2}$ and $w(z)$ is the $1/e^2$ intensity radius of the beam given by:

$$w(z) = w_0\sqrt{1 + \left(\frac{z - z_0}{z_R}\right)^2}. \tag{2}$$

Here w_0 is the beam waist, z_0 is the focal point and z_R is the Rayleigh range given by $z_R = \pi w_0^2/\lambda_T$. An atom in the presence of a light field has its energy levels perturbed. The ground state ac stark shift is:

$$U(r, z) = -\frac{\alpha_0}{2\epsilon_0 c} I(r, z), \tag{3}$$

where α_0 is the ground state polarizability. For Rb and $\lambda_T = 1064\,$nm, Safronova *et al* [19] calculate $\alpha_0 = (4\pi\epsilon_0) \times 693.5 a_0^3\,\mathrm{C\,m^2\,V^{-1}}$, where a_0 is the Bohr radius. A 19 W laser with a

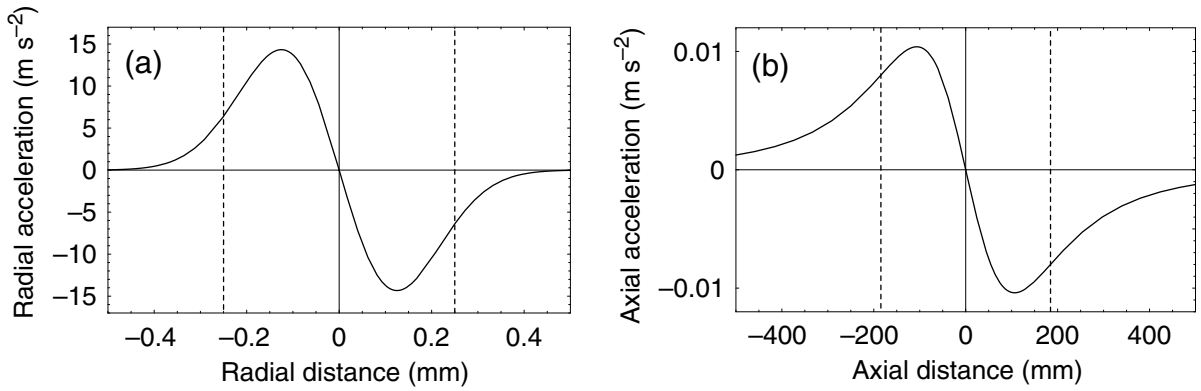

Figure 2. (a) Radial and (b) axial accelerations plotted against distance from the beam centre. A 19 W laser with beam waist of 250 μm is used in the calculation. The radial acceleration is $\sim 10^3$ times larger than the axial case. The dashed vertical lines in (a) and (b) are $\pm w_0$ and $\pm z_R$ respectively.

beam waist of 250 μm (peak intensity of 1.94×10^8 W m^{-2}) produces a maximum trap depth of $U/k_B = 30.2\,\mu$K. The effect of heating due to light scattering is negligible. Calculations for the above parameters give a scattering rate of $\sim$0.1 photons per second.

When in the presence of a laser beam, the atoms experience a dipole force, $\vec{F}(r, z) = -\nabla U(r, z)$, due to the spatial variation of the laser potential. The radial and axial accelerations for a ^{85}Rb atom have been plotted in figure 2. The radial acceleration is comparable with g and three orders of magnitude larger than the axial case. It is sufficiently large to provide an adequate guide for the cold atoms. In contrast, one would not expect to see much evidence of perturbation from the ballistic motion in the axial direction. The length scales over which the radial and axial accelerations change are characterized by the beam waist and the Rayleigh range respectively. The radial angular frequency for the laser guide is given by:

$$\omega_{r_L} = \sqrt{\frac{4\alpha_0 P}{m\epsilon_0 c\pi\, w(z)^4}}. \tag{4}$$

2.3. Loading the guide

Calculating the guiding efficiency can be broken down into two separate problems: loading atoms from the MOT into the guide and subsequent transport losses. The fraction of atoms initially captured by the laser beam can be calculated analytically based on the work of Pruvost *et al* [2] and extended by Wolschrijn *et al* [20]. An atom will be radially bound if its total energy E is less than zero:

$$E = \frac{p^2}{2m} + U(r, z) < 0, \tag{5}$$

where $p = \sqrt{p_x^2 + p_y^2}$ is the radial momentum and m is the atomic mass. The initial atom distribution can therefore be divided into two groups: energetically bound ($E < 0$) and unbound

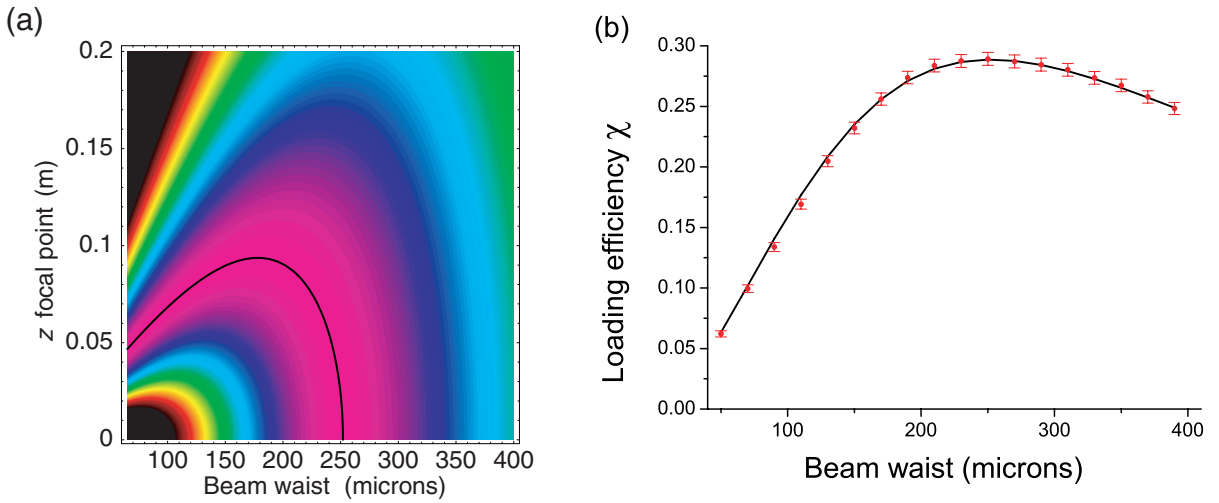

Figure 3. (a) The analytical load efficiency, χ, plotted against beam waist and z focal point. The black contour represents the optimum $1/e^2$ beam radius of 252 μm which corresponds to a load efficiency of 28.9%. (b) The $z_0 = 0$ cross section of (a). The solid line is the analytical result and the data points are the result of a numerical simulation consisting of 10 000 atoms.

($E > 0$). The normalized initial position and momentum distribution of the atomic cloud for a given temperature $\mathcal{T}$ is given by:

$$\Phi(r, p) = \frac{\mathrm{e}^{-r^2/2{\sigma_R}^2}}{2\pi{\sigma_R}^2} \frac{\mathrm{e}^{-p^2/2mk_\mathrm{B}\mathcal{T}}}{2\pi mk_\mathrm{B}\mathcal{T}}. \tag{6}$$

The loading efficiency, χ, is calculated by integrating $\Phi(r, p)$ and imposing the bound condition of equation (5) as the momentum integration limit:

$$\chi = 4\pi^2 \int_0^\infty \int_0^{\sqrt{2mU(r,z)}} \Phi(r, p) rp \,\mathrm{d}r \,\mathrm{d}p. \tag{7}$$

By using the substitution $q = \mathrm{e}^{-2r^2/w(z)^2}$ for the second integral, the solution is:

$$\chi = 1 - \frac{w(z)^2}{4\sigma^2} \left(\frac{\alpha_0 P}{\epsilon_0 c\pi w(z)^2 k_\mathrm{B}\mathcal{T}} \right)^{-(w(z)^2/4\sigma^2)} \Gamma\left(\frac{w(z)^2}{4\sigma^2}, 0, \frac{\alpha_0 P}{\epsilon_0 c\pi w(z)^2 k_\mathrm{B}\mathcal{T}} \right), \tag{8}$$

where $\Gamma(a, b, c) = \int_b^c q^{a-1}\mathrm{e}^{-q}\,\mathrm{d}q$ is the generalized incomplete gamma function. The loading efficiency is plotted against beam waist and focal point in figure 3(a). The optimum $1/e^2$ radius for loading the modelled experiment is 252 μm, and that produces a load efficiency of 28.9%. The maximum exhibits a large plateau ($\chi > 25\%$ when the $1/e^2$ radius is between 175 and 360 μm) which results in flexibility in choosing initial parameters. Due to this flexibility, we have chosen to study laser guiding when the beam focus coincides with the MOT centre ($z_0 = 0$ cm). The reason for this is that an expanding beam will cool the cloud in the radial direction during the flight [2]; this is a consequence of Liouville's theorem. Unless otherwise stated, the results presented will

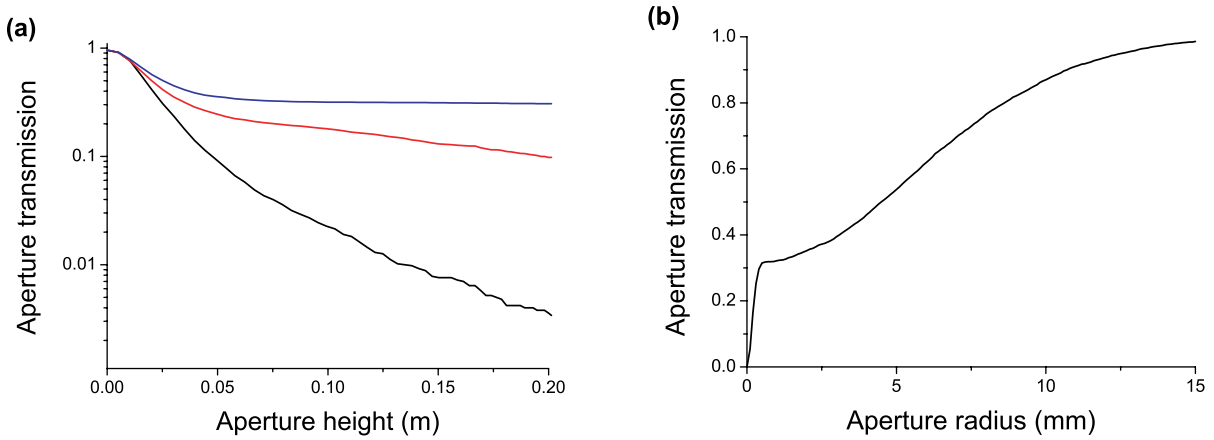

Figure 4. (a) Aperture transmission plotted against aperture height above the MOT centre for a 0.5 mm radius aperture. The black line is with no laser present, the red line is with a laser of waist 100 μm and the blue line is with a 250 μm waist. (b) The transmission fraction plotted against aperture radius for an aperture at a height of 18.0 cm above the MOT. The distribution consists of a tightly guided core due to a laser of waist 250 μm and the ballistically expanded cloud ($\sigma_r = 5.4$ mm). The simulation follows the trajectories of 5000 atoms to obtain the aperture transmission.

use a laser that is focused on the MOT centre ($z_0 = 0$), see figure 3(b). Alongside the analytical result a Monte Carlo simulation of atomic trajectories was performed by solving the equations of motion that include gravity and the dipole force. The data points on the plot show the fraction of atoms from the MOT that are initially energetically bound and therefore satisfy equation (5).

The loading efficiency can be increased by using a more powerful laser, a lower temperature atomic cloud or a smaller cloud size. The first two are intuitively obvious, however the reduction in cloud size is misleading because atom number is the important experimental quantity we wish to maximize. For a MOT with constant atom density, the atom number increases proportional to the cube of the cloud radius. Although for large clouds a smaller cloud fraction is loaded, there is a greater number of atoms present and therefore the overall load increases with cloud radius.

2.4. Transport losses

Having considered the initial loading of the MOT into the laser beam, attention is now turned to the guiding properties and losses from the beam. Apart from heating and collisions (which are assumed to be negligible) there are two loss mechanisms: aperture truncation and diffraction.

2.4.1. Truncation losses. Without laser guiding the transmission from a ballistically expanded cloud passing through a 0.5 mm radius aperture at a height of 18 cm is 0.4%. With guiding this transmission can be increased by 75 times. This is shown in figure 4(a) where the transmission through the aperture is plotted against height above the MOT. The black line represents the transmission of an unguided atomic cloud. The aperture height of 18.0 cm was chosen to minimize ballistic transmission but still allow sufficient distance between the aperture and trajectory apex at 22 cm. The red and blue lines demonstrate laser guiding for 100 μm and 250 μm beam waists

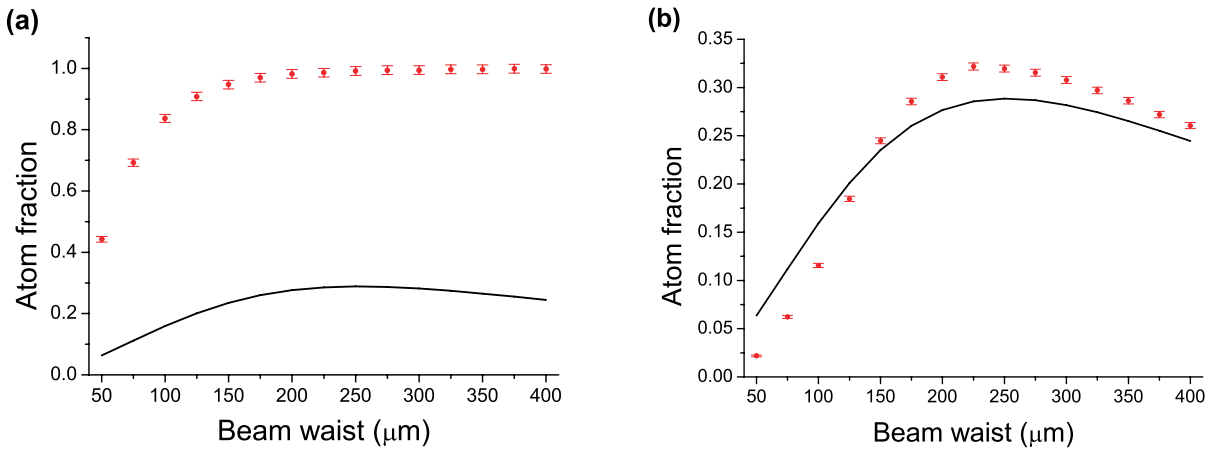

Figure 5. (a) The ratio of the number of energetically bound atoms at the aperture to the number of initially bound atoms plotted against beam waist. Values less than one represent losses due to diffraction. (b) The fraction of atoms passing through the aperture plotted against beam waist. the quantity represents the overall transport efficiency. The solid line in both plots is the loading efficiency χ given by equation (8).

respectively. Again there is the initial decay due to the unguided atoms passing through the aperture. However unlike the unguided case, a fraction of the atoms have been bound in the laser guide which significantly increases the aperture transmission. This corresponds to the tight core evident in figure 1(b). There is also atom loss from the guide due to diffraction. This is more obvious in the tightly focused 100 μm beam (red line), although all expanding laser beams will suffer losses. This diffraction loss is examined in subsubsection 2.4.2.

In figure 4(b), there is a plot of transmission versus aperture radius at 18.0 cm above the MOT centre. The sharp spike in the distribution is due to the guided atoms and the broader distribution is due to the ballistically expanded atomic cloud. The aperture size should be large enough to allow the guided atoms to pass through unhindered. The highest achievable loading efficiency for the setup modelled has a beam radius of $w(z) = 349\ \mu$m at the aperture. The $1/e^2$ radius is twice the radial standard deviation: $w(z) = 2\sigma_r$. With this definition, the beam radius is $\sigma_r = 175\ \mu$m and therefore the 0.5 mm aperture has a radius of $2.86\sigma_r$, corresponding to a 99.6% transmission through the aperture. A much larger beam radius could result in high losses when passing through the small aperture.

2.4.2. Diffraction losses. Away from the focus, diffraction causes the guiding potential to relax. For some bound atoms this can mean their kinetic energy becomes larger than the depth of the confining potential—the atoms are therefore lost from the guide. Ideally a transportation scheme requires a laser profile that does not change size on the scale of the guiding distance. The Rayleigh length is a good measure of this, and therefore for efficient guiding one must ensure that the transport distance is on the order or less than the Rayleigh length. A Monte Carlo simulation of 5000 atoms being transported within the laser guide was run to investigate the loss due to diffraction. In figure 5(a) the red data points are the ratio of the number of energetically bound atoms at the aperture to the number of initially bound atoms. For small beam waists, the

Rayleigh length is much smaller than the transport length and the increased diffraction reduces the transport efficiency.

The overall transport efficiency is shown in figure 5(b). In this plot, the fraction of atoms passing through the aperture is plotted against beam waist. In addition to the fraction of bound atoms passing through the aperture (obtained by multiplying the two curves in figure 5(a)), there is an extra contribution from nearly bound atoms that have been 'funnelled' through the aperture. Those nearly bound were either just outside the bound criteria of equation (5) at the initial MOT loading, or have been lost from the guide due to diffraction. Their trajectories loosely follow the laser guide, and therefore there is an increased probability of passing through the aperture. Simulations show that the distribution of unbound atoms that are transmitted through the aperture peaks at 6%, which accounts for the extra 4% contribution to the transport efficiency curve in figure 5(b). The peak in the unbound atom distribution is centred at a smaller beam waist, due to the unbound atoms having a hotter temperature than their bound counterparts. This explains why the transport efficiency curve has its peak shifted to 225 μm.

It is instructive to look at phase-space plots to get an understanding of the initial capture and subsequent loss due to diffraction, see figure 6. The left (right) column simulates a laser with a 100 μm (250 μm) beam waist. The diffraction of the laser beam can be seen by studying the evolution of the dashed $E = 0$ contour. The 250 μm beam provides a better guide as it both captures more atoms initially and suffers from less diffraction loss. In both plots, the nearly bound atoms can be seen just outside the $E = 0$ line. It takes a finite time for them to be ejected from the guide. It is these atoms that are the extra contribution in figure 5(b).

3. Magnetic focusing theory

Laser guiding is an ideal method to deliver cold atoms with a tight radial distribution, however it does not address the problem of the expanding axial distribution. In previous work, we studied and optimized the focusing properties of pulsed magnetic lenses made from current-carrying coils [13, 14]. In this paper, we investigate four different lens designs that can focus the cloud in the axial direction while radial confinement is provided by the laser guide. This section provides a summary of the key results needed to understand pulsed magnetic focusing, a comprehensive explanation can be found in the publications cited above.

3.1. The Stern–Gerlach force

A full description of the Stern–Gerlach force relevant to atomic lenses can be found in subsection 2.1 of [13]. In brief, for atoms optically pumped into either a strong-field-seeking (SFS) state with magnetic moment μ_B (the Bohr magneton), or into a weak-field-seeking (WFS) state with magnetic moment $-\mu_B$, the Stern–Gerlach force is $\vec{F}_{SG} = \pm\mu_B \nabla B$—i.e. the focusing of the atoms is governed by the gradient of the magnetic field magnitude only. It should be noted that the guiding properties within the laser beam are independent of the atom's magnetic moment at such large detunings.

3.2. Magnetic fields from current-carrying coils

A purely harmonic magnetic field magnitude will result in an aberration-free lens. Such a field can be closely approximated with the use of current-carrying circular coils. The fields are constrained

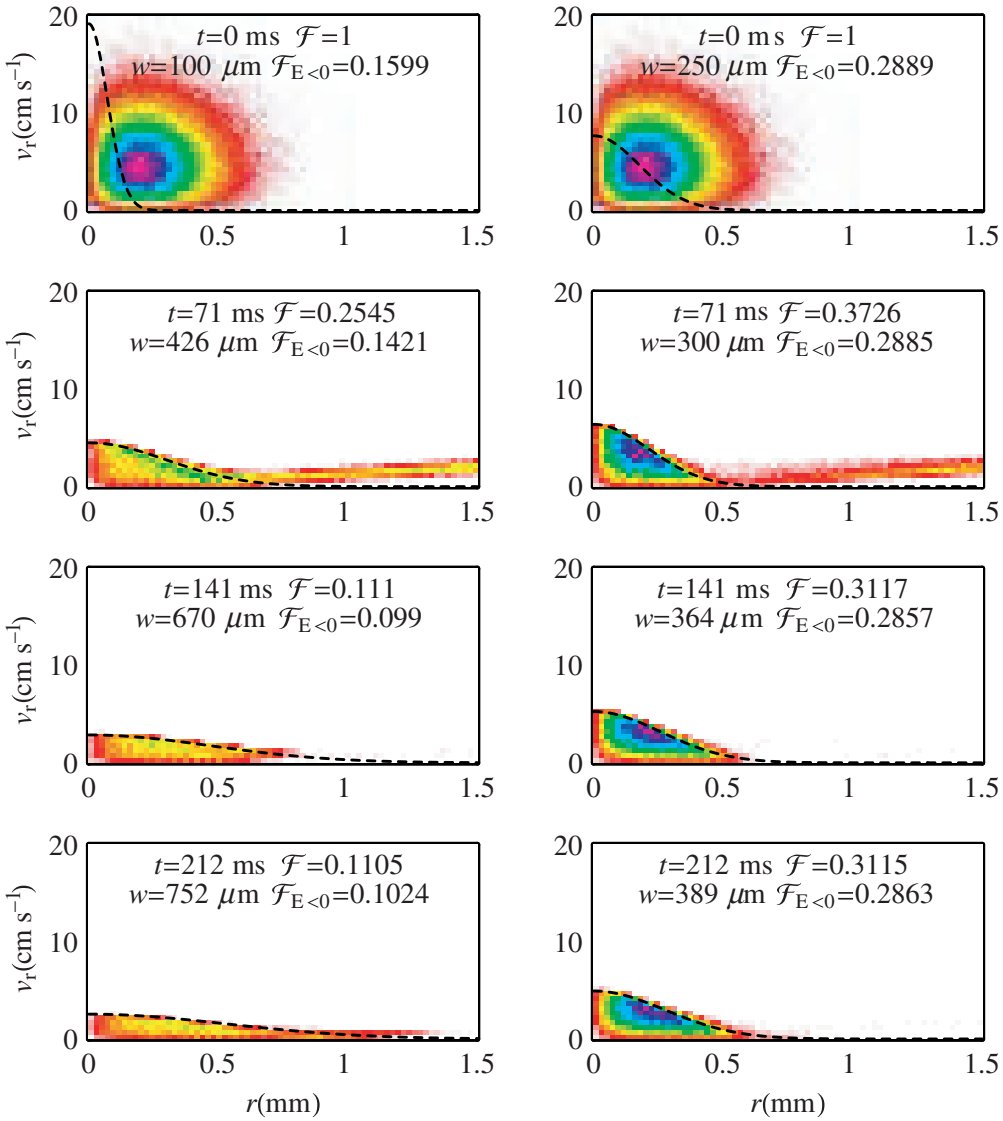

Figure 6. Phase-space plots (radial velocity v_r versus radial position r) of 10^5 atoms in a laser guide with a 100 μm (left column) and 250 μm (right column) beam waist. Dashed lines are the $E = 0$ energy contours, and $\mathcal{F}$ ($\mathcal{F}_{E<0}$) is the visible (bound and visible) atom fraction. See also supplementary gif movies of the phase-space dynamics for a dipole guide with a 100 μm beam waist (rv_r or rz) and a 250 μm beam waist (rv_r or rz). The aperture is indicated by a line in one frame of the rz movie, and in rv_r by a line at $r = 0.5$ mm when the atom cloud centre-of-mass is within three cloud standard deviations of the aperture.

by Maxwell's equations, which, in conjunction with symmetry arguments, allow the spatial dependence of the fields to be parameterized with a small number of terms. A cylindrically symmetric magnetic coil configuration has second-order magnitude:

$$B(r, z) = B_0 + B_1(z - z_c) + \tfrac{1}{2}B_2(z - z_c)^2 + \frac{1}{4}\left(\frac{{B_1}^2}{2B_0} - B_2\right)r^2, \tag{9}$$

where B_0, B_1 and B_2 are the bias field, the axial gradient and the field curvature, respectively. The point $\{0, 0, z_c\}$ defines the centre of the lens.

Consider two coils of N turns with radius a, separation s, carrying currents I_1 and I_2. It is convenient to partition the currents in each coil as a current I_H with the same sense and a current I_{AH} in opposite senses, i.e. $2I_H = I_1 + I_2$, $2I_{AH} = I_1 - I_2$. We define $\eta = \mu_0 NI/2$, and use the scaled separation $S = s/a$.

3.2.1. Axially asymmetric lenses. When $\eta_{AH} \neq 0$ there is no axial symmetry and therefore B_{odd} terms are present. A purely axial lens with no third-order terms can be created by ensuring $B_3 = 0$ and ${B_1}^2 = 2B_0B_2$. In practice this is achieved by setting $S = \sqrt{3}$ and $\eta_{AH} = \pm\frac{4}{3}\eta_H$, (see subsection 2.2 in [13]), which corresponds to $I_1/I_2 = -7$ or $-1/7$. The existence of the axial gradient B_1, corresponds to the addition of a constant acceleration along the z-axis during the magnetic pulse:

$$a_0 = \frac{\mu_B B_1}{m} = \frac{3\mu_B \eta_{AH} S}{ma^2(1 + S^2/4)^{5/2}}. \tag{10}$$

The direction in which the acceleration acts depends upon whether the current flow is larger in the higher or lower coil. A useful measure of the lens' strength is the square of the angular frequency. For this design $\omega_r^2 = 0$ and the axial strength is given by:

$${\omega_z}^2 = \frac{\mu_B B_2}{m} = \frac{6\mu_B \eta_H (S^2 - 1)}{ma^3(1 + S^2/4)^{7/2}}. \tag{11}$$

For WFS (SFS) atoms the magnetic coils act as a converging (diverging) lens. For the transport scheme under investigation, therefore one must ensure that atoms are prepared in the WFS state. Such a lens will be referred to as an 'axial-only lens' henceforth.

3.2.2. Axially symmetric lenses. In the case of an axially symmetric system ($\eta_{AH} = 0$) there is a simplification as $B_{odd} = 0$. There is now a nonzero curvature in the radial direction, which is related to axial curvature via ${\omega_r}^2 = -{\omega_z}^2/2$. From equation (11), when $S < 1$ the lens has negative curvature along the z-axis, and therefore a SFS atom is focused and a WFS is defocused; the opposite is true for $S > 1$. The harmonicity of a SFS (WFS) converging lens is optimized if $S = 0.58$ ($S = 2.63$). These converging lenses will be referred to as a 'SFS lens' and a 'WFS lens' henceforth.

3.3. Pulse timing

For a given lens of strength ω^2, the calculation of the pulse start time, t_1, and duration, τ, required to bring the atomic cloud to a focus at a time T is not trivial. The finite pulse time means the atom's position and velocity will be modified during the pulse and therefore the simple focusing formulae of 'thin lens' optics cannot be used. A full description of the timing requirements can be found in subsection 4.3 of [13]. A mathematical transformation can be made from the lab frame of 'thick lenses' to 'thin lenses':

$$\tau'(\omega, \tau) = \frac{2}{\omega}\tan\frac{\omega\tau}{2}, \qquad t_1' = t_1 + \tau'/2, \qquad T' = T - \tau + \tau'. \tag{12}$$

Table 1. The focusing properties are tabulated for the 5 cm magnetic lenses studied in this paper. The pulse duration has been calculated for a pulse occurring at $\lambda = 0.5$. The accelerating and decelerating axial-only lenses from subsubsection 3.2.1 are shown in rows 1 and 2. The SFS and WFS lenses from subsubection 3.2.2 are shown in rows 3 and 4. A complex angular frequency corresponds to negative curvature and hence defocusing.

	S	NI_1 (A)	NI_2 (A)	a_0(m s^{-2})	ω_r (rad s^{-1})	ω_z (rad s^{-1})	τ (ms)
Axial-only	$\sqrt{3}$	−1429	10 000	+121	0	49	11.6
lenses	$\sqrt{3}$	10 000	−1429	−121	0	49	6.6
SFS lens	0.58	10 000	10 000	0	70i	100	1.9
WFS lens	2.63	10 000	10 000	0	42i	59	5.5

The notation of primes is used to denote times in the 'thin' lens representation. In the limit of a short, strong pulse $\omega\tau \to 0$, we find that $\tau' \to \tau$. We define a dimensionless parameter to represent the timing of the lens pulse:

$$\lambda = \frac{t_1'}{T'}, \tag{13}$$

which yields a magnification of $(\lambda - 1)/\lambda$. The required pulse duration to achieve focusing is obtained by solving:

$$\omega T' \sin \omega\tau = \frac{1}{\lambda(1-\lambda)}. \tag{14}$$

4. Laser guiding and magnetic focusing

This section will investigate the axial focusing of atomic clouds being guided within a laser beam with a beam waist of 250 μm. The choice of lens radius is a compromise between a strong lens with short pulse durations (small radius) and a weak lens with low aberrations (large radius). Aberrations arise as a consequence of the departure from a parabolic profile of the lens' potential. A 5 cm radius lens has sufficiently low aberrations and short enough pulse durations so as to avoid coil heating, therefore results for a 5 cm radius lens will be presented in this paper. The lens properties are tabulated in table 1 for the four different lens designs studied. An experimental limit on the maximum current flowing in the coils was set at $NI = 10\,000$ A. It is interesting to contrast the radial angular frequency of the lens with that of the laser guide. From equation (4) and the laser parameters above, the initial radial angular frequency in the $w = 250\,\mu$m laser guide is $\omega_{r_L} = 435$ rad s^{-1}. Therefore in the radial direction the laser will dominate over the magnetic field's influence.

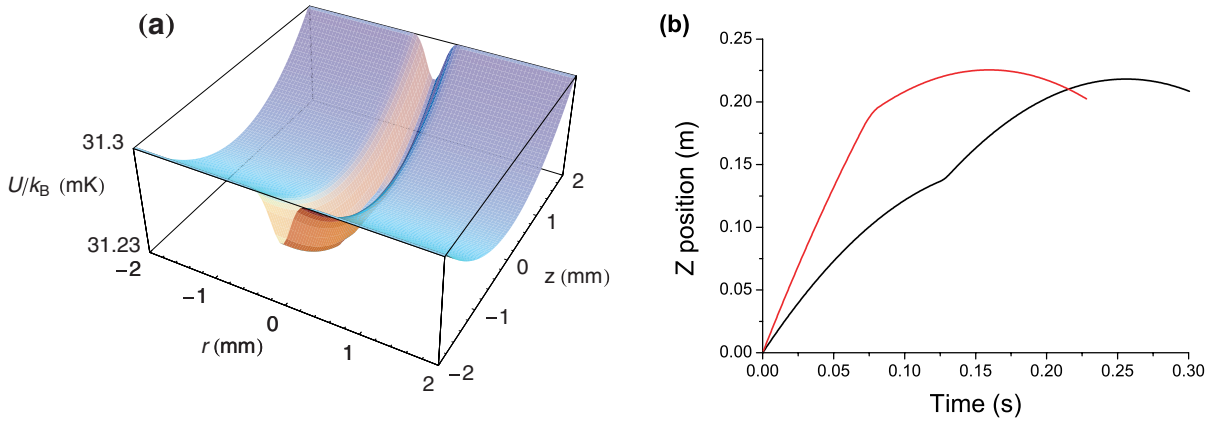

Figure 7. (a) The potential energy surface of the combined laser and axial-only magnetic lens. The lens has a radius of 5 cm and carries a maximum current of $NI = 10\,000$ A. The B_1 term has been subtracted to show the focusing properties of the lens. (b) The atomic cloud centre of mass' vertical position plotted against time for a decelerating (red line) and an accelerating (black line) axial-only lens. The magnetic pulse occurs at $\lambda = 0.5$. The decelerating (accelerating) lens requires a faster (slower) launch velocity and the flight time is shorter (longer).

4.1. Axial only focusing

The use of a lens that does not perturb the radial motion would seem an ideal candidate for combining with a laser guide. In figure 7(a) the combined laser and the full magnetic field potential using elliptic integrals has been plotted. The constant B_1 term has been subtracted to emphasize the axial curvature and lack of radial curvature. For realistic lens parameters the constant acceleration's magnitude is on the order of 100 m s^{-2}. Typically the acceleration changes the cloud's vertical velocity by about 1 m s^{-1}. Depending on the lens' orientation this can either slow or accelerate the atomic cloud's flight, see figure 7(b). The initial launch velocity has to be modified to take this change into account so that the cloud apex remains at the required height. As an aside, it should be noted that the ability to accelerate or decelerate a cloud could have uses in a horizontal transport scheme as a means to modify the centre of mass motion.

Based upon a simple trajectory model that incorporates three stages of acceleration ($-g$ when $\{0 < t < t_1\}$ and $\{t_1 + \tau < t < T\}$; $a_0 - g$ when $\{t_1 < t < t_1 + \tau\}$), and ensuring that the centre of mass comes to rest at a height h, the required launch velocity is:

$$v_{z_i} = a_0\tau + \sqrt{g(2h + a_0(t_1 + \tau)(t_1 - \tau))}, \tag{15}$$

and the apex time of such a flight path is:

$$T = \frac{v_{z_i} - a_0\tau}{g}. \tag{16}$$

As expected when $a_0 = 0$ these return to the free-flight launch velocity $v_{z_i} = \sqrt{2gh}$ and apex time $T = \sqrt{2h/g}$. Ensuring that the focus occurs at the same time as the cloud's apex is nontrivial. The pulse length is calculated based upon knowledge of the required focus time, see equation (14).

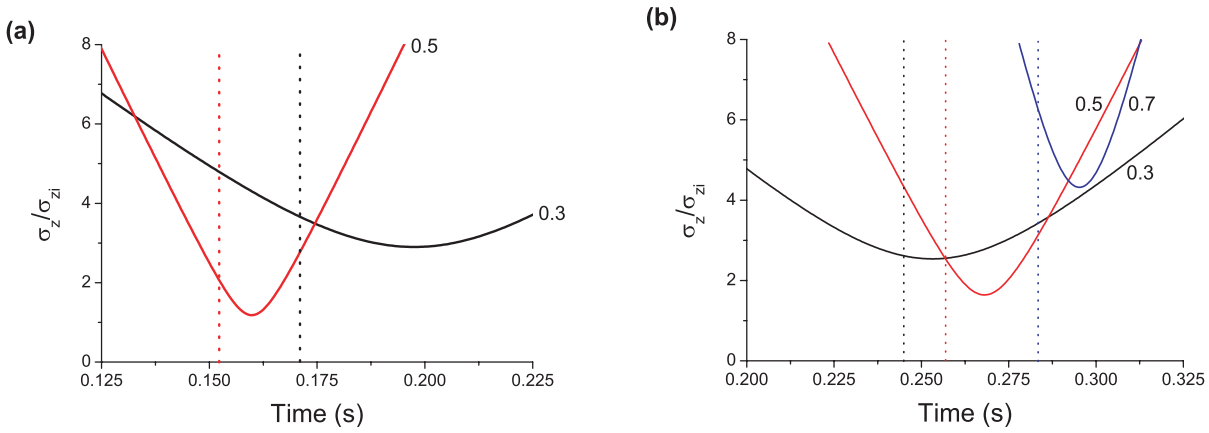

Figure 8. The change in axial cloud standard deviation, σ_z/σ_{z_i}, plotted against time for (a) a decelerating and (b) an accelerating 5 cm radius axial-only lens. Three lens positions are plotted: $\lambda = 0.3$ (black line), 0.5 (red line) and 0.7 (blue). The radial confinement was provided by a 19 W laser guide with a beam waist of 250 μm. The vertical lines indicate the predicted focus times—the colours matching the corresponding line.

But the focus time depends upon the location, duration and strength of the magnetic pulse. Solving the problem requires iteration.

A further complication arises in the case of a decelerating lens due to the fact that the vertical launch velocity, v_{z_i}, can become complex for some t_1 and τ values. The physical situation that corresponds to this case is where the desired apex height has been reached before the pulse has finished. One finds that this limits the maximum λ that can be used. The situation is worse for larger radius lenses as these require longer pulse durations to achieve focusing. The accelerating lens does not suffer from this kind of upper bound on λ.

With the radial confinement being provided by the laser field, focusing is only required in the axial direction, hence the investigation becomes one-dimensional. The quality of the focus was investigated, and figure 8 plots the change in axial standard deviation, σ_z/σ_{z_i}, against time for different values of λ. There is no $\lambda = 0.7$ line for the decelerating lens for the reason explained in the previous paragraph. Neither lens causes magnetic pulse losses from the laser guide. For both decelerating and accelerating 5 cm lenses the minimum cloud size is achieved for $\lambda = 0.5$, resulting in a change in axial standard deviation of 1.18 and 1.64 respectively. If the lenses were free of aberrations, one would expect to see no change in axial size at the focus (i.e. $\sigma_z/\sigma_{z_i} = 1$). An unfocused cloud's axial size would have increased by a factor of 34 and 59 respectively. The aberrations of the axial-only lens inhibit achieving a compressed image.

4.2. Axial focusing/radial defocusing lenses

The effect of significant aberrations and the complication of the constant acceleration for axial-only lenses are undesired. These can be avoided by allowing the radial direction to be perturbed with either the SFS or WFS lenses described in subsubsection 3.2.2. The combined potential resulting from the magnetic and laser fields is shown in figure 9(a). At the centre, the optical dipole potential dominates and there is positive curvature causing focusing in all three spatial

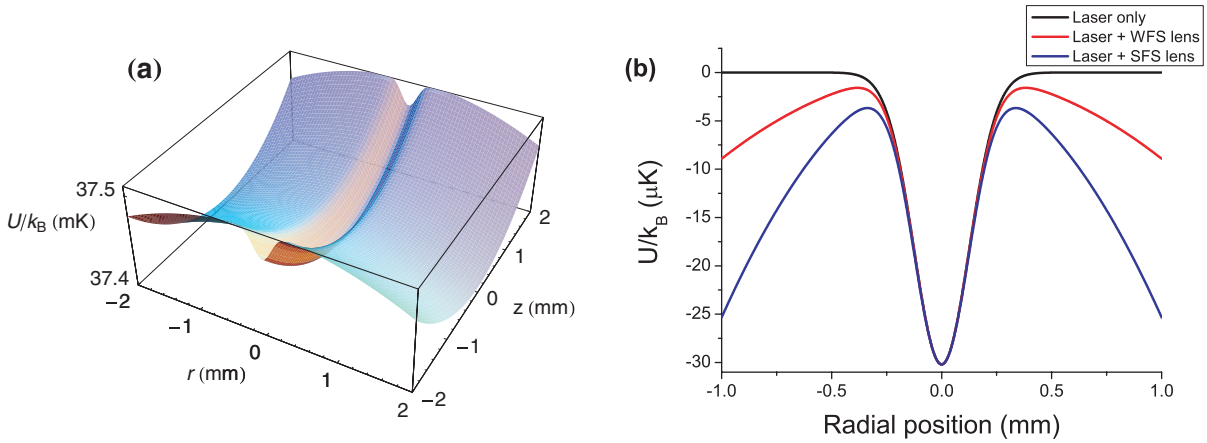

Figure 9. (a) The potential energy surface of the combined laser and magnetic fields for a WFS lens plotted against radial and axial position. The laser has a beam waist of 250 μm and the lens has a radius of 5 cm and $NI = 10\,000$ A. In (b) the cross section along the $z = 0$ line is plotted. The black line is the laser only potential, the red line is the combined laser and magnetic potential for a WFS lens and the blue line is the combined potential for a SFS lens. For a WFS (SFS) lens the trap depth is 95% (88%) of the laser depth. Note: the combined potentials have offsets added so that the three minima coincide.

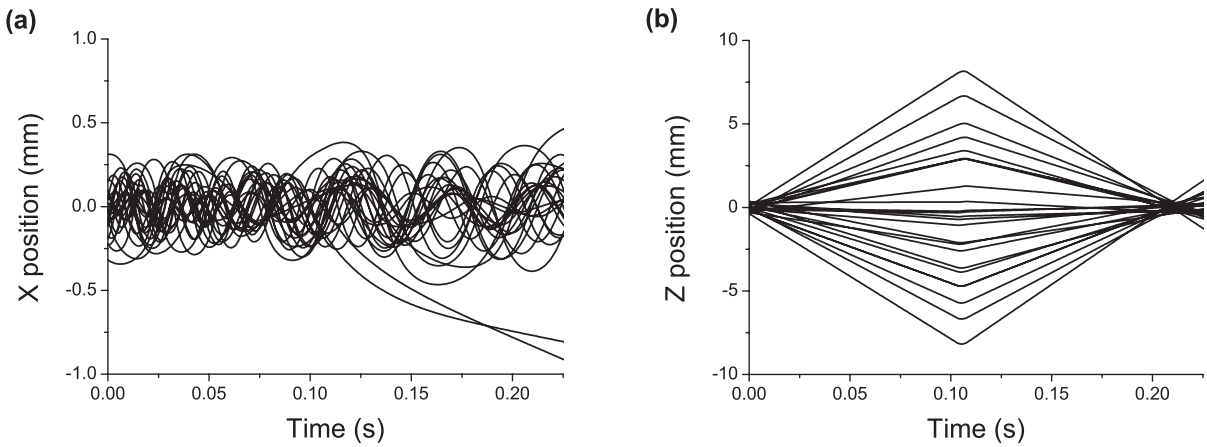

Figure 10. The trajectories of 25 atoms are simulated passing through the laser guide and being focused by a 5 cm radius WFS lens. The pulse occurs at $\lambda = 0.5$ and has a duration of 5.5 ms. Plot (a) shows the x-axis position and plot (b) the z-axis position relative to the cloud's centre of mass.

directions. However, away from the z-axis the magnetic potential becomes significant and the radial curvature turns negative. This turn over is shown more clearly in the $z = 0$ cross section in figure 9(b). The trap depth has been reduced, which means some atoms will have become energetically unbound during the lens pulse, see equation (5).

In figure 10 the trajectories of 25 atoms are plotted in the centre of mass frame for (a) the radial direction and (b) the axial direction. In this example a 5 cm WFS lens was positioned at

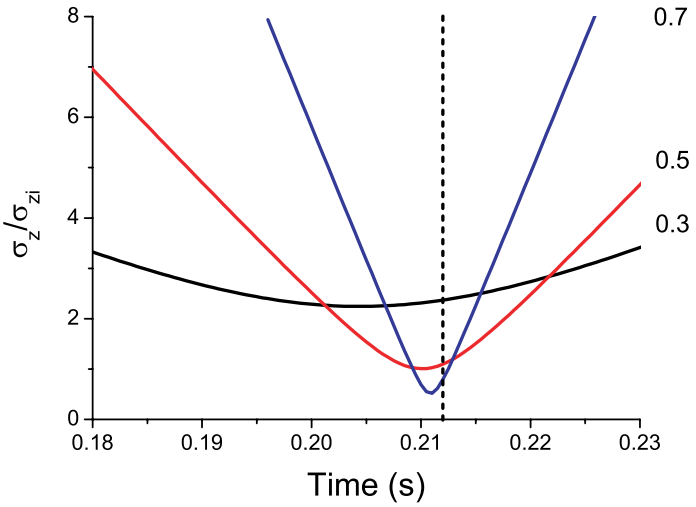

Figure 11. The change in the cloud's axial standard deviation, σ_z/σ_{z_i}, plotted against time for a WFS lens. Three lens positions are plotted: $\lambda = 0.3$ (black line), 0.5 (red line) and 0.7 (blue), the minimum change is 2.2, 1.0 and 0.5 respectively. The expected minima based upon the magnification $(\lambda - 1)/\lambda$ are 2.33, 1.00 and 0.43 respectively. The dashed vertical line indicates the predicted focal time of 212 ms.

$\lambda = 0.5$ and was pulsed on for 5.5 ms to bring the cloud to a focus at the fountain apex. In this simulation two atoms were lost as a result of the magnetic lens pulse. Before investigating the quality of the focused cloud, attention is turned to characterising these pulse losses.

If an atom's velocity is not modified, the 'window of opportunity' to escape only lasts as long as the pulse time, which is usually of the order of a few milliseconds. This escape time is short compared to the radial oscillation period within the laser guide. The period is obtained from equation (4): $T_{\rm osc} = 2\pi/\omega_{r_{\rm L}}$. For a 19 W laser with $1/e^2$ radius of 250 μm this corresponds to a period of 14 ms. Therefore an individual atom will only perform $\sim$1/10th of an oscillation and is unlikely to escape. One would expect the loss due to this mechanism to scale with the pulse duration τ. However, the magnetic pulse modifies the velocity of the atoms. For some atoms this can result in them becoming energetically unbound both during and after the pulse. Over time these unbound atoms will escape from the guide. The loss due to the magnetic pulse was measured to be $\sim$2%, and is tiny compared with the loss associated in the initial loading of the laser guide.

We now address the focusing properties of the SFS and WFS magnetic lenses. For small radius lenses, aberrations tend to dominate resulting in a poor focus and unpredictable focus time. When the lens radius is increased above 5 cm for a WFS lens ($S = 2.63$) and above 7 cm for a SFS lens ($S = 0.58$), no further improvements are observed. The $S = 0.58$ lens suffers from worse aberrations as the atoms experience more of the anharmonic B-field due to their closer proximity to the coils.

In figure 11 the change in axial standard deviation, σ_z/σ_{z_i}, for a 5 cm WFS lens is plotted against time for different values of λ. The effect of aberrations is significantly less for this design

Table 2. The change in the atomic cloud's properties (position standard deviation σ, aspect ratio ξ, velocity standard deviation σ_v and temperature $\mathcal{T}$) for different transportation schemes. The columns are as follows: the initial cloud properties generated in the MOT; the cloud loaded from the MOT into a 250 μm beam waist laser guide; a cloud that has been transported within the laser guide to the 22 cm apex; a guided cloud that has been focused by a decelerating axial-only lens; a guided cloud that has been focused by an accelerating axial-only lens; a guided cloud that has been axially focused by a SFS lens; a guided cloud that has been axially focused by a WFS lens. Each lens has a radius of 5 cm, a maximum current of $NI = 10\,000$ A and is pulsed on at $\lambda = 0.5$, see table 1.

	MOT	Bound atoms	Apex	$-a_0$ axial only lens	$+a_0$ axial only lens	SFS lens	WFS lens
σ_x (mm)	0.20	0.11	0.19	0.19	0.19	0.22	0.21
σ_z (mm)	0.20	0.20	9.4	0.37	0.66	0.22	0.21
$\xi = \sigma_z/\sigma_r$	1.00	1.81	50	1.96	3.57	1.03	0.99
σ_{vx} (cm s^{-1})	4.42	2.53	1.67	1.63	1.68	1.71	1.71
σ_{vz} (cm s^{-1})	4.42	4.41	4.40	3.93	4.03	4.42	4.47
$\mathcal{T}_x$ (μK)	20	7	3	3	3	3	3
$\mathcal{T}_z$ (μK)	20	20	20	16	17	20	20

compared with an axial-only lens. The minima are only slightly worse than values achievable with an aberration-free lens. For the case of $\lambda = 0.7$ the cloud is compressed along the axial direction to half of its initial size. Unlike previous work where aberrations dominate a similar plot at high λ (see figure 6 in [13]), we find that for laser guided atoms this is not the case. This is due to the strong radial confinement provided by the laser guide.

4.3. Transported cloud properties

Numerical simulations were performed to compare different transportation schemes. The position and velocity standard deviations of the atomic cloud were computed after tracing the trajectories of individual atoms. The results are presented in table 2. For ease of comparison the equivalent temperature, $\mathcal{T}$, corresponding to a given velocity and the cloud aspect ratio, $\xi = \sigma_z/\sigma_r$, are also tabulated. It should be noted that when the cloud is trapped in the upper chamber, the temperature will rethermalize via collisions. The trap geometry will determine the rethermalized temperature.

5. Discussion and conclusion

5.1. Lens comparison

The performances of the different lenses are encapsulated in table 2. The first column shows the properties of the initial MOT. The second gives the properties of that atoms loaded into the guide. As expected these have a smaller radial extent, and as only the least energetic are loaded,

a lower radial temperature. For the launched atoms with only laser guiding (third column) there is a slight increase in the radial size as a consequence of the laser beam diffracting, and the axial size grows by more than an order of magnitude. The cloud has a very elongated sausage shape ($\xi \gg 1$). Focusing the laser guided cloud with either a decelerating or an accelerating axial-only lens (columns four and five respectively) produces a radial extent similar to an unfocused laser guided cloud, however the axial extent is significantly smaller than with no magnetic lens, but not as compact as the original launched cloud. This is a consequence of the aberrations associated with this lens design. The last two columns characterize the performance of optimized SFS and WFS lenses. Although there is a slight atom loss during the impulse associated with the negative radial curvature, the performance of these lenses is far superior, yielding moderately larger radial clouds, and one-to-one axial imaging. In all cases the slight increase of the radial extent is accompanied by a concomitant reduction of the radial temperature, a manifestation of Liouville's theorem.

While initially it appears as if axial-only lenses would complement the radial laser guiding, the results of the simulations shows that the best strategy would be to use optimized harmonic WFS or SFS lenses. The axial-only lens is harder to realize experimentally, and as a consequence of the broken axial symmetry, has more significant aberrations. However, it can be used without further atom loss during the magnetic impulse. By contrast the optimized harmonic SFS and WFS lenses do suffer a slight atom loss during the pulse. However this is insignificant compared to the initial loading loss. The axial-focusing of these two lenses is superior, and the simulations show that for realistic experimental parameters better than one-to-one axial focusing could be achieved when $\lambda > 0.5$.

There is a slight broadening of the cloud radially, arising from the laser beam's increased width. It might be possible to circumvent this by 'zooming' a lens such that the centre of mass of the atom cloud is always confined by the tightest focus of the beam. This would keep the initial cloud confined to the same final radial width. However this would be at the expense of significant experimental complexity.

5.2. The 'ultimate' density

An important feature of any new technique is to determine how much of an improvement can be achieved. We now compare the maximum density increase that can be achieved using either a dipole guide alone or a combination of a magnetic lens and an identical dipole guide. The maximum density increase during guiding will be approximately the fraction of atoms guided times the decrease in cloud volume (i.e. the square of the radial decrease in cloud size times the axial decrease in cloud size).

To maximize the guided atom fraction, we need to choose the dipole waist at the MOT ($z = 0\,\mathrm{cm}$) near the range $w = 175$–$360\,\mu\mathrm{m}$ (from subsection 2.3). To maximize the radial compression of the MOT we try to minimize the waist at the apex ($z = 22\,\mathrm{cm}$) compared to the waist at the MOT ($z = 0\,\mathrm{cm}$). Two sensible strategies are: (a) the guide beam waist $w_0 = 193\,\mu\mathrm{m}$ at $z_0 = 11\,\mathrm{cm}$ a Rayleigh range from both the apex and MOT ($w = \sqrt{2}w_0 = 273\,\mu\mathrm{m}$ at $z = 0,\ 22\,\mathrm{cm}$); (b) the beam waist $w_0 = 273\,\mu\mathrm{m}$ at the apex $z_0 = 22\,\mathrm{cm}$, a Rayleigh range from the MOT ($w = \sqrt{2}w_0 = 386\,\mu\mathrm{m}$ at $z = 0\,\mathrm{cm}$). There is only a 10% difference in final density between the methods and we chose the option with higher final density (b) as the larger radial compression outweighs the higher loading loss.

Table 3. The fraction of atoms focused, the relative density increase radially, the relative density increase axially and the overall density increase are shown for the dipole guide only and for the combination of dipole guide and a magnetic lens. With the parameters optimized for the largest density increase an order of magnitude improvement over the initial atom cloud is achieved with the dipole guide and lens.

Guide type	$\mathcal{F}^f$	ρ_r^f	ρ_z^f	ρ^f
Dipole guide only	0.270	1.67	0.0213	0.0160
Dipole guide + magnetic lens	0.227	1.68	15.8	10.2

We have chosen a SFS lens with $S = \sqrt{3-\sqrt{7}} \approx 0.595$, instead of $S = 0.58$, as guided atoms have only a small amount of radial expansion and one can therefore concentrate on minimising the axial anharmonicities in the lens potential [13]. The maximum value of λ and hence the smallest axial focus that can be achieved using a pulse of duration τ from a lens with angular frequency ω during the total atomic guiding time T is the solution of the nonlinear expression: $\omega(\tau_{\max} - T) = \tan \omega\tau_{\max}$ [13]. For $S = 0.595$ using the coil radius 5 cm and current 10 000 A from table 1, we have $\omega = 97.5\,\mathrm{rad\,s^{-1}}$ and $\tau_{\max} = 16.6\,\mathrm{ms}$ which leads to an effective focal time $\lambda = 0.950$ and thus an axial magnification of $-1/19.5$ for a purely harmonic lens.

By using 2D Gaussian fits to the binned Monte Carlo data in rz space we extract information about the atomic distribution at the focus $t \approx T + 12\,\mu$s: the fraction of atoms $\mathcal{F}^f$ focused as well as the relative density increases in the radial direction ρ_r^f, axial direction ρ_z^f and overall $\rho^f = \mathcal{F}^f(\rho_r^f)^2\rho_z^f$. The results are encapsulated in table 3.

We have made movies to compare the phase space dynamics of a dipole guide alone (left images in movies) and a dipole guide combined with an $S = 0.595$ maximum duration ($t = T - \tau_{\max} \to t = T$) magnetic lens (right images in movies). Phase-space movies in rv_r, rz, zv_z and v_rv_z are available. The rv_r movie shows how the magnetic lens almost exclusively removes the funnelled atoms with $E > 0$. A dramatic difference in final atomic density at the apex of the atomic motion is seen in the rz movie. The aberrations in the magnetic lens are illustrated by the 'Z' shaped zv_z focus (the horizontal bars of the 'Z' are the high axial velocity atoms which experience the anharmonic regions of the magnetic lens). The concomitant increase in axial velocity with an increase in axial density [14] is illustrated in the zv_z and v_rv_z movies.

5.3. Conclusions

In summary, we have analysed the loading and guiding of a fountain of vertically launched atoms by a far detuned laser beam. Although the optical dipole force provides strong radial confinement, the axial width of the cloud grows by more than a order of magnitude. A hybrid approach using the optical dipole force for radial confinement and the Stern–Gerlach force for pulsed axial focusing was analysed, and found to yield total density increases of an order of magnitude—almost three orders of magnitude greater than by a dipole guide alone.

Acknowledgments

This work is supported by EPSRC, the UKCAN network and Durham University. SLC acknowledges the support of the Royal Society. We thank Charles Adams, Simon Gardiner and Kevin Weatherill for fruitful discussions.

References

[1] Szymaniec K, Davies H J and Adams C S 1999 *Europhys. Lett.* **45** 50–55
Davies H J, Szymaniec K and Adams C S 2000 *Phys. Rev.* A **62** 013412
Davies H J and Adams C S 2000 *J. Phys. B: At. Mol. Opt. Phys.* **33** 4079–86
[2] Pruvost L, Marescaux D, Houde O and Duong H T 1999 *Opt. Commun.* **166** 199–209
[3] Noh H R, Xu X and Jhe W 2002 *Adv. At. Mol. Opt. Phys.* **48** 153–90
[4] Renn M J, Montgomery D, Vdovin O, Anderson D Z, Wieman C E and Cornell E A 1995 *Phys. Rev. Lett.* **75** 3253–6
Renn M J, Donley E A, Cornell E A, Wieman C E and Anderson D Z 1996 *Phys. Rev.* A **53** R648–51
Renn M J, Zozulya A A, Donely E A, Cornell E A and Anderson D Z 1997 *Phys. Rev.* A **55** 3684–96
Ito H, Sakaki K, Ohtsu M and Jhe W 1997 *Appl. Phys. Lett.* **70** 2496–8
[5] Gustavson T L, Chikkatur A P, Leanhardt A E, Görlitz A, Gupta S, Pritchard D E and Ketterle W 2002 *Phys. Rev. Lett.* **88** 020401
[6] Dowling J P and Gea-Banacloche J 1996 *Adv. At. Mol. Opt. Phys.* **37** 1–94
Balykin V I 1999 *Adv. At. Mol. Opt. Phys.* **41** 181–260
[7] Hinds E A and Hughes I G 1999 *J. Phys. D: Appl. Phys.* **32** R119
[8] Roach T M, Abele H, Boshier M G, Grossman H L, Zetie K P and Hinds E A 1995 *Phys. Rev. Lett.* **75** 629
Sidorov A I, McLean R J, Rowlands W J, Lau D C, Murphy J E, Walciewicz M, Opat G I and Hannaford P 1996 *Quantum Semiclass. Opt.* **8** 713
Lau D C, Sidorov A I, Opat G I, McLean R J, Rowlands W J and Hannaford P 1999 *Eur. Phys. J.* D **5** 193
Lev B, Lassailly Y, Lee C, Scherer A, Mabuchi H 2003 *Appl. Phys. Lett.* **83** 395
Hughes I G *et al* 1997 *J. Phys. B: At. Mol. Opt. Phys.* **30** 647
Hughes I G *et al* 1997 *J. Phys. B: At. Mol. Opt. Phys.* **30** 2119
Hughes I G *et al* 2001 *J. Phys. B: At. Mol. Opt. Phys.* **34** 2869
Saba C V *et al* 1999 *Phys. Rev. Lett.* **82** 468
Rosenbusch P *et al* 2000 *Phys. Rev.* A **61** 031404
Rosenbusch P *et al* 2000 *Appl. Phys.* B **70** 709
Kadio D, Houde O and Pruvost L 2001 *Europhys. Lett.* **54** 417
[9] Bloch I, Köhl M, Greiner M, Hänsch T W and Esslinger T 2001 *Phys. Rev. Lett.* **87** 030401
Arnold A S, MacCormick C and Boshier M G 2002 *Phys. Rev.* A **65** 031601(R)
Arnold A S, MacCormick C and Boshier M G 2004 *J. Phys. B: At. Mol. Opt. Phys.* **37** 485
[10] Cornell E A, Monroe C and Wieman C E 1991 *Phys. Rev. Lett.* **67** 2439
[11] Marechal E, Guibal S, Bossennec J L, Gorza M P, Barbe R, Keller J C and Gorceix O 1998 *Eur. Phys. J.* D **2** 195
Marechal E, Guibal S, Bossennec J L, Barbe R, Keller J C and Gorceix O 1999 *Phys. Rev.* A **59** 4636
Miossec T, Barbe R, Keller J-C and Gorceix O 2002 *Opt. Commun.* **209** 349
[12] Smith D A, Arnold A S, Pritchard M J and Hughes I G *In preparation*
[13] Pritchard M J, Arnold A S, Smith D A and Hughes I G 2004 *J. Phys. B: At. Mol. Opt. Phys.* **37** 4435
[14] Arnold A S, Pritchard M J, Smith D A and Hughes I G 2006 *New J. Phys.* **8** 53
[15] Greiner M, Bloch I, Hänsch T W and Esslinger T 2001 *Phys. Rev.* A **63** 031401

[16] Lewandowski H J *et al* 2003 *J. Low Temp. Phys.* **132** 309
Goldwin J, Inouye S, Olsen M L, Newman B, DePaola B D and Jin D S 2004 *Phys. Rev.* A **70** 021 601(R)
Nakagawa K *et al* 2005 *Appl. Phys.* B **81** 791–94
[17] Lahaye T, Reinaudi G, Wang Z, Couvert A and Guéry-Odelin D 2006 *Phys. Rev.* A **74** 033622
[18] Lett P D, Phillips W D, Rolston S L, Tanner C E, Watts R N and Westbrook C I 1989 *J. Opt. Soc. Am.* B **6** 2084–2107
[19] Safronova M S, Williams C J and Clark C W 2004 *Phys. Rev.* A **69** 022509
[20] Wolschrijn B T, Cornelussen R A, Spreeuw R J C, van Linden van den Heuvell H B 2002 *New J. Phys.* **4** 69